Periostin Regulates Collagen Fibrillogenesis and the Biomechanical Properties of Connective Tissues

Russell A. Norris,[1]* Brook Damon,[2] Vladimir Mironov,[1] Vladimir Kasyanov,[3] Anand Ramamurthi,[1,4] Ricardo Moreno-Rodriguez,[1] Thomas Trusk,[1] Jay D. Potts,[5] Richard L. Goodwin,[5] Jeff Davis,[5] Stanley Hoffman,[1] Xuejun Wen,[1] Yukiko Sugi,[1] Christine B. Kern,[1] Corey H. Mjaatvedt,[1] Debi K. Turner,[1] Toru Oka,[6] Simon J. Conway,[7] Jeffery D. Molkentin,[6] Gabor Forgacs,[2] and Roger R. Markwald[1]

[1]Department of Cell Biology and Anatomy, Medical University of South Carolina, Charleston, South Carolina
[2]Department of Physics and Astronomy, University of Missouri-Columbia, Columbia
[3]Riga Stradins University, Riga LV-1007, Latvia
[4]Department of Biomedical Engineering, Clemson University, Clemson, South Carolina
[5]Department of Cell and Developmental Biology and Anatomy, University of South Carolina, Columbia, South Carolina
[6]Department of Molecular Cardiovascular Biology, Children's Hospital Medical Center, Cincinnati, Ohio
[7]Wells Center for Pediatric Research, Indiana University School of Medicine, Indianapolis, Indiana

Abstract Periostin is predominantly expressed in collagen-rich fibrous connective tissues that are subjected to constant mechanical stresses including: heart valves, tendons, perichondrium, cornea, and the periodontal ligament (PDL). Based on these data we hypothesize that periostin can regulate collagen I fibrillogenesis and thereby affect the biomechanical properties of connective tissues. Immunoprecipitation and immunogold transmission electron microscopy experiments demonstrate that periostin is capable of directly interacting with collagen I. To analyze the potential role of periostin in collagen I fibrillogenesis, gene targeted mice were generated. Transmission electron microscopy and morphometric analyses demonstrated reduced collagen fibril diameters in skin dermis of periostin knockout mice, an indication of aberrant collagen I fibrillogenesis. In addition, differential scanning calorimetry (DSC) demonstrated a lower collagen denaturing temperature in periostin knockout mice, reflecting a reduced level of collagen cross-linking. Functional biomechanical properties of periostin null skin specimens and atrioventricular (AV) valve explant experiments provided direct evidence of the role that periostin plays in regulating the viscoelastic properties of connective tissues. Collectively, these data demonstrate for the first time that periostin can regulate collagen I fibrillogenesis and thereby serves as an important mediator of the biomechanical properties of fibrous connective tissues. J. Cell. Biochem. 101: 695–711, 2007. © 2007 Wiley-Liss, Inc.

Key words: periostin; collagen; fibrillogenesis; connective tissues; fasciclin

---

Collagen Type I is a main structural protein of the extracellular matrix (ECM), responsible for the mechanical properties of fibrous connective tissues such as cornea, tendon, ligaments, blood vessels, and heart valves. Alterations in collagen biosynthesis, assembly, and cross-linking are involved in the pathogenesis of a broad spectrum of connective tissue diseases such as Marfan syndrome and Ehlers-Danlos Syndrome (EDS) [Scarbrough et al., 1984; Loughlin et al., 1995; Burrows et al., 1996; Wang et al., 1996; Bonnet et al., 1997; Milewicz, 1998; von Kodolitsch et al., 1998; Pyeritz, 2000; Loeys et al., 2001; Elcioglu et al., 2004; Peeters et al., 2004; Schwarze et al., 2004; Lindor and Bristow,

2005; Robinson et al., 2006]. In vivo collagen fibrillogenesis is a complex, developmentally regulated, multistep process involving many collagen associated proteins, pericollagen proteins, and proteoglycans [Birk and Trelstad, 1986; Canty and Kadler, 2002, 2005; Kadler, 2004]. It has been shown that certain ECM proteins such as tenascin-X [Minamitani et al., 2004a,b], sparc [Bradshaw et al., 2003], fibronectin [Li et al., 2003], thrombospondin [Kyriakides et al., 1998; Bornstein et al., 2000; Bradshaw et al., 2003] as well as proteoglycans, such as decorin [Zhang et al., 2006], byglycan [Ameye and Young, 2002; Ameye et al., 2002], lumican [Matheson et al., 2005], and fibromodulin [Ezura et al., 2000; Chakravarti, 2002; Goldberg et al., 2006] regulate collagen fibrillogenesis and thereby the mechanical properties of connective tissues. In addition to these matrix proteins, we demonstrate that members of the fasciclin gene family (i.e., *periostin*) also appear to play essential roles in regulating this process.

Periostin is a secreted 90 kDa ECM protein, related to the midline fasciclin-1 (mfas-1) gene in Drosophila [Horiuchi et al., 1999]. The family of fasciclin genes in mammals is relatively small comprising four highly related members: periostin, βIG-H3, stabilin-1, and stabilin-2. Periostin is strongly expressed in collagen-rich fibrous connective tissues subjected to constant mechanical stresses in vivo, such as the periodontal ligament (PDL), the periosteum, endocardial cushions, the mature cardiac valves, and their supporting structures in the developing heart [Kruzynska-Frejtag et al., 2001, 2004; Sasaki et al., 2001; Wilde et al., 2003; Katsuragi et al., 2004; Litvin et al., 2004; Norris et al., 2004, 2005; Kern et al., 2005; Lindsley et al., 2005; Nakamura et al., 2005]. Expression of periostin is significantly increased in response to mechanically regulated BMP and TGFβ growth factor signaling in mesenchymal cells undergoing differentiation [Horiuchi et al., 1999; Li et al., 2005; Lindner et al., 2005].

Gene targeted periostin null mice have recently been generated and support the potential role of periostin in regulating biomechanical properties of connective tissues [Rios et al., 2005; Kii et al., 2006]. These mice show a severe incisor enamel defect, suggesting that periostin is required for the integrity, absorption of mechanical stresses, and anchorage of the ameloblast cell lineage. The absence of periostin

protein leads to defects in ameloblast morphology and results in the secretion of abnormal and unstructured matrix and altered enamel formation, ultimately resulting in enhanced tooth wear [Rios et al., 2005]. Furthermore, periostin null mice show an eruption disturbance of incisors which is attributed to the disappearance of the shear zone [Kii et al., 2006]. This is due, in part, to the failure of proper collagen fiber turnover. These results suggested that periostin may function in the remodeling of the collagen matrix in the shear zone of PDLs [Kii et al., 2006]. The mechanisms by which periostin affect collagen synthesis, remodeling, maturation, and stabilization have only been hypothesized. Therefore, more elaborate studies are needed to determine the significance that the putative periostin−collagen connection may have in developing and maintaining functional connective tissues. Recent evidence has supported an interaction of periostin with other ECM molecules such as fibronectin, tenascin-C, and collagen V [Takayama et al., 2006]. However, no detailed investigations have been reported on putative interactions between periostin and collagen I, as well as how this molecular interaction may significantly affect the biomechanical properties of connective tissues.

In this report, we demonstrate for the first time that periostin is co-localized with collagen Type I and directly binds to collagen Type I. How this interaction is of functional significance was further evaluated in the context of periostin null mice and in periostin overexpression experiments. An evaluation of collagen I fibrillogenesis in the skin of *periostin* null mice demonstrated a reduction in collagen fibril diameter resulting in a decrease in overall stiffness. In addition, differential scanning calorimetry (DSC) experiments demonstrated a significant reduction in collagen cross-linking, a defect associated with improper collagen fibril formation. On the other hand, when periostin was overexpressed in cardiac valvulogenic tissue, the overall viscosity, a measure of collagen cross-linking was increased. Collectively, these data indicate that periostin is essential for proper collagen fibril formation and maturation. This is the first report on the molecular interactions of periostin with collagen Type I and validates periostin as an important regulator of collagen fibrillogenesis. More importantly, proper biomechanical

function of connective tissues, such as heart valves, skin, and tendon are dependent on this collagen I-periostin interaction.

MATERIALS AND METHODS

Animals: Mouse

Breeding pairs of 3-month-old periostin −/− knockout and wild-type mice derived from sv129 line (manuscript in preparation) were housed in a fully accredited American Association for Accreditation of Laboratory Animal Care (AAALAC) facility and the Medical University of South Carolina' institutional animal care and use committee approved all experiments. All animals were classified as either periostin knockout or wild-type by PCR genotyping of genomic DNA isolated from tail clips. Primers used in genotyping were: upper: 5′-ccttgccagtctcaatgaagg-3′, lower WT- 5′-tga-cagagtgaacacatgcc, lower KO- 5′-ggaagacaatag-caggcatg. Cycling conditions were: 100°C (2 min), 96°C (2 min), 30 cycles of 96°C (35 s), 56°C (35 s), 72°C (75 s) with a final extension of 72°C (5 min). Periostin null and wild-type age matched mice (3 months of age) were used for analysis. Only male mice were used in these experiments.

Animals: Chicken

One hundred twenty fertilized viral-free chicken eggs (Spafas) were incubated for 6 days in a humidity controlled 37°C incubator. After 6 days, HH27 embryos were removed, washed in PBS, and hearts were isolated. Further dissection of the hearts was performed to isolate atrioventricular (AV) valve tissues, which were used as explants for adenoviral infection experiments as described below.

Histochemistry

Left AV valve leaflets were isolated from adult mouse hearts. The leaflets were fixed with 3.5% formaldehyde in PBS for 2 h, then methanol for 2 h, rehydrated and stained for collagen using picrosirius red as previously reported in Whittaker et al. [1994].

Immunohistochemistry (IHC)

Three-month-old mouse tissue was fixed in 4% paraformaldehyde (skin) or 100% cold methanol (hearts), embedded in paraffin, and sectioned at 5 μm. Deparaffinized sections were rehydrated through a graded series of ethanol to PBS. IHC on skin sections was performed as previously described [Kern et al., 2005]. IHC on heart valve sections was performed similarly except that blocking was performed for 15 min in 10% NGS/1% BSA/PBS. Sections were incubated with the primary antibody (rabbit anti-mouse periostin-1:100 dilution) and washed with 1% BSA/PBS. Negative controls for IHC were performed by incubation with normal rabbit IgG in place of the primary antibody. The specificity of this antibody has previously been evaluated by us and [Rios et al., 2005] with no detectable expression or non-specific cross-reactivity present in the context of the periostin null background (data not shown). Heart sections were double immunostained with the muscle marker, MF20 (1:1 antisera). No appreciable staining was observed in negative controls for periostin (data not shown). Immunostained sections were viewed with a Leica TCS SP2 AOBS Confocal Microscope System.

Immunogold Transmission Electron Microscopy

Hearts were dissected from adult C57Bl6 mice and sectioned transversely. Sections containing AV valve leaflets were then processed for TEM. Samples were fixed in 2% paraformaldehyde/0.1% glutaraldehyde (PBS) overnight at 4°C. Samples were then dehydrated in increasing concentrations of EtOH at −20°C and embedded in Lowicryl K4M (EMS) with UV polymerization for 48 h. Further curing was carried out under ambient fluorescence lighting until clear (∼2 weeks). Cured blocks were cut on a Leica UltraCut R microtome and 110 nm sections were collected on nickel mesh grids. Grids were blocked with PBS solutions containing 0.05 M glycine, 1% CWFS gelatin, and 5% BSA. Grids were then incubated overnight in 1:50 dilution of the rabbit anti-mouse periostin antibody (660 ng/ml) at 4°C. No primary antibody controls were incubated in a solution of 1% BSA/0.05% Tween-20/PBS. After rinsing, these grids were incubated for 2 h with a 1:25 dilution of the goat anti-rabbit 10 nm gold conjugate anti sera (EMS) in 1% BSA (PBS). The grids were then fixed with 1% glutaraldehyde (PBS), and stained with 0.25% OsO4 (aq). Grids were stained with 2% uranyl acetate and Hanaichi lead stain prior to viewing on a JEOL 200CX transmission electron microscope at 120 kV.

Adenoviral Generation

A full-length mouse periostin cDNA was obtained from Dr. Simon Conway (Indiana University-Purdue University Indianapolis) and cloned into the pDNR-CMV shuttle vector (Clontech). To facilitate detection of the virally produced protein, a hemagluttinin (HA) tag (YPYDVPDYA) was inserted at the carboxyl-terminus through standard PCR techniques. The mouse periostin cDNA insert and the proximal CMV promoter were moved into the Adeno-X Acceptor Vector through a Cre/Lox mediated recombination. DNA from positive transformants was isolated and transfected into HEK293 cells. Infectious viral particles were purified using the Adeno-X Viral Purification Kit (Clontech). Titers for both periostin viruses were determined by plaque assays and spectrophotometry to be $1-2 \times 10^9$ pfu/ml. Two control viral constructs expressing the β-galactosidase (LacZ) gene and GFP were also generated in this same manner.

Cell Culture and Western Analysis

1×10^5 HEK293 cells were plated on tissue culture plastic and infected with either the periostin or LacZ adenoviruses at an MOI of five. After 2 days the cells and supernatant were removed. The cell and supernatant mixture was spun at $1,000 \times$ rpm for 10 min. to pellet the cells. Supernatant was removed and the cells were lysed in a $1 \times$ RIPA buffer (with and without 100 mM β-mercaptoethanol reducing agent) with mild sonication. Both supernatant and cell lysates were stored at $-20°C$. Total protein from the cell lysate was quantified (Pierce-Commassie Protein Assay). Twenty microgram of cell lysate and 20 μl of infected media were loaded on a 4–15% SDS–PAGE. Proteins were electroblotted onto nitrocellulose membranes and immuno-probed for periostin expression using an α-HA antibody (1:1,000 in 5% milk-Sigma HA-7 clone) followed by a goat α-mouse-HRP (1:7,500 in 5% milk) secondary antibody (Sigma). Immunopositive bands were detected by ECL (Pierce) and autoradiography. Western analysis of periostin expression in wild-type, heterozygous, and homozygous skin samples were accomplished similarly as described above with minor differences (Fig. 1). Skin samples were dissected and snap frozen in liquid nitrogen. Frozen samples were fractured and ground up by mortar and pestle.
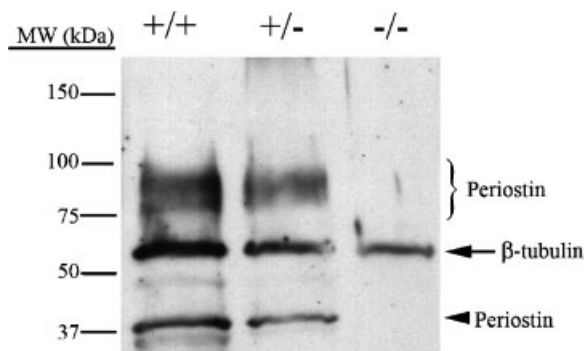

Fig. 1. Western verification of periostin knockout mice. Protein lysates were generated from skin biopsies from wild-type (+/+), heterozygous (+/−), and periostin null mice (−/−), and subjected to Western analysis for periostin expression. Expression of periostin isoforms is seen around the predicted 90–100 kDa and the 37 kDa molecular weights. The heterozygotes decrease in total periostin expression by roughly half and no expression is detected in the periostin nulls. β-tubulin was used as a normalization control.

This process was repeated and followed by the addition of a $1 \times$ RIPA buffer. Western analysis of periostin expression was accomplished as described previously. In house rabbit α-mouse periostin antibody was used at a 1:2,500 dilution

Transmission Electron Microscopy and Fibril Diameter Analysis

The dorsal skin from age-matched wild-type and periostin−/− mice was dissected out. The dorsal skin was immersed in 2% glutaraldehyde (TAAB, UK) and processed for transmission electron microscopy. Briefly, samples were rinsed and post-fixed in 1% osmium tetroxide (Merck, NJ) in 0.1 M cocadylate buffer, and thereafter dehydrated in graded acetones and embedded in Epon (Electron Microscopic Sciences). Ultrathin sections were stained with 3% uranyl acetate and 0.2% lead citrate, and were examined under a JEOL electron microscope (JEOL, Japan). At least four mice of each genotype were used for measurement of collagen fibril diameter and distribution. Micrographs (four per group) from non-overlapping regions of the dorsal skin were taken from cross-sections. The distribution of collagen fibril diameters was calculated using NIH image. Eight areas in a square were chosen from dorsal skin of each genotype for determination of distribution.

Co-Immunoprecipitation and Western Blotting of Collagen and Periostin

Thirty microliters Protein-A agarose beads (Sigma) bound with an antibody to rat tail collagen I (Abcam) were blocked for 1 h at 37°C in 1% BSA/1XTBST. Block was removed and the complexes were incubated overnight at 4°C with 5 μg of purified rat tail collagen I (BD Biosciences). Collagen complexes were spun (3 min at 6,000g), washed (5× in TBST), and resuspended in 500 μl periostin infected HEK 293 serum-free conditioned media. Complexes were incubated at RT for 2 h, then spun, and washed 5× in TBST. Binding complexes were dissociated by addition of either a 1× SDS non-reducing loading buffer or a 1× SDS denaturing loading buffer (containing 100 mm β-mercaptoethanol) and boiled at 95°C for 5 min. Eluates were run on a 4–20% SDS–PAGE and immunoblotted using an α-HA antibody (Sigma HA-7 Clone) 1:500 in 5% milk, 1× TBST. A rabbit α-mouse-HRP secondary (Sigma 1:5,000) was used followed by ECL detection (Pierce). As a control, subsequent staining of the IP plot was performed with an α-rabbit collagen I antibody (1:1,000 Abcam).

AV Valve Explant Adenoviral Infections

Fertilized white leghorn eggs (Spafas, Inc., Roanoke, IL) were incubated at 38.5°C with 80% humidity until the desired Hamburger Hamilton developmental stage was reached, HH27~5 days [Hamburger and Hamilton, 1951]. Chicken AV valve explants were isolated from HH27 embryos and incubated overnight in hanging drop cultures (DMEM/10% FBS/100 UPen/Strep) with 6×10^6 PFUs of mouse periostin virus. A portion of these hanging drops were used in Western analysis to verify viral infection whereas others were used for measuring tissue surface tension (described below).

Measurement of Tissue Surface Tension

Tissue surface tension (a quantitative measure of the apparent liquid properties of embryonic tissues) of periostin infected and LacZ control infected chicken valve tissues was determined as described previously [Foty et al., 1996; Forgacs et al., 1998]. Briefly, isolated AV chicken embryo HH27 valve explants were rounded overnight and placed into a tensiometer (Fig. 9A). The compression apparatus (modified from previously used similar devices [Forgacs

et al., 1998] used in this work to measure the liquid tissue properties is shown in Figure 9. A typical measurement was performed as follows. Spheroidal aggregates, ranging in diameter from 200 to 300 μm, were placed on the lower plate of the apparatus in CO_2 independent medium (with 100 U pen/strep; GIBCO/BRL) at 37°C, and rapidly compressed with the help of a stepping motor to produce a deformation of a definite magnitude. To minimize adhesion of the aggregate to the compression plates, these were coated with poly-2 hydroxyethylmethacrylate (polyHEMA). To avoid irreversible damage to the cells, aggregates were compressed a maximum of 30% of their original diameter. The time variation of the force exerted by the explant upon the upper compression plate was measured using a Cahn/Ventron (model 2000, Cerritos, CA) electrobalance (the upper compression plate was connected to the arm of the balance). The force relaxation process was recorded by Labview software (National Instruments, Austin, TX) until the compressive force reached a constant equilibrium value (45–60 min), at which point the plates were separated, and the aggregate was allowed to regain its original shape. Measurements in the rare cases when the aggregate did not regain its pre-compressed shape were discarded. The shape of the aggregate before, during, and after compression, was recorded by a Spot Insight CCD camera (Diagnostic Instruments, Sterling Heights, MI) fitted to a horizontally positioned dissecting microscope (SZ60, Olympus). The surface tension of the model tissue was evaluated using the Laplace equation [Forgacs et al., 1998]: $F_{eq}/(\pi R_3^2) = \sigma(1/R_1 + 1/R_2)$. Here σ is the tissue's apparent surface tension (i.e., interfacial tension with the surrounding tissue culture medium), F_{eq} is the equilibrium value of the compressive force, R_3 is the radius of the circular contact area of the compressed aggregate with the plates. R_1 and R_2 are the radii of curvature of the aggregate's surface, respectively, along its equatorial plane, and its peripheral contour, which is assumed to be circular. The geometric parameters were determined by an in-house built tracking program, with a precision of 3 μm. The program evaluates the aggregate's recorded contour on the basis of variation in gray scale values in its vicinity. To check tissue liquidity (i.e., the independence of σ on the compressive

force) aggregates were compressed 2–3 times with varying force with 60 min recovery in uncompressed state. Average σ values were calculated from at least six independent measurements.

Valve Tissue Explant Fusion Assays

The viscosity of cushion tissue was determined from the time (t) variation of the circular interfacial area (of instantaneous radius R) between two similar-size fusing roundup explants. According to the theory of viscous liquids the length parameter $L = (2/3)\pi(R^2/R_0)$ varies as $L = (\sigma/\eta)t$, where R_0 and η are, respectively, the radius of the unfused explants and tissue viscosity [Frenkel, 1945].

DSC to Determine Levels of Collagen Cross-Linking

Freshly isolated tendon samples from periostin knockout (n = 5) and wild-type mice (n = 5), weight ranging from 5 to 8 μg, were sealed, respectively, in aluminum pans and their DSC thermograms were recorded on Mettler Toledo DSC 822e calorimeter with temperature increments of 5°C/min).

Biomechanical Analysis

To investigate the influence of periostin on collagen fiber cross-linking, pieces of skin from the dorsal side of wild-type males (n = 6) and periostin null male (n = 3) mice were used as experimental material. Prior to skin biopsies, hair from the dorsal part of mice was removed by a hair remover gel "Nair" (Carter-Horner Corp., Mississauga, ON, Canada). In order to perform tensile tests, rectangular shaped dorsal skin samples (50 mm long and 4.5 mm wide in the middle) oriented parallel to the spine was dissected with the aid of a dual-bladed surgical knife. The specimens were kept in M199 medium (Sigma) at room temperature (20°C) and tested within 1 h of sacrifice. Before measurements were obtained, skin samples were placed between two microscope slides, and overall thickness of the specimens was measured with a micrometer device "Ultra Digital Mark IV" (Fowler, Swiss) with accuracy of ±0.001 mm. Specimens were gripped between specially designed "alligator" clamps to prevent slippage of the tissue, and tensile tests were performed using MTS materials testing system (Synergie 100) with a load cell of 50 N. Force-elongation curves were recorded at a constant elongation rate of 5 mm/min until failure. During experimentations, the skin specimens were kept continuously moist with room temperature M199 media. Stress was calculated from force in Newton (N) divided by the initial cross-section area of the specimen. Incremental modulus of elasticity between the levels of stress 0.25/0.3 MPa of samples was calculated also using MTS provided software.

Statistical Analysis

Results are displayed as the mean ± standard deviation. One-factor analysis of variance (ANOVA) was utilized to evaluate mechanical properties and intergroup comparison by means of a Student's t-test using a difference of $P < 0.05$.

RESULTS

Periostin is expressed in collagen rich fibrous connective tissues subjected to high levels of mechanical loading [Horiuchi et al., 1999; Kruzynska-Frejtag et al., 2001, 2004; Oshima et al., 2002; Beck et al., 2003; Wilde et al., 2003; Katsuragi et al., 2004; Kudo et al., 2004; Litvin et al., 2004, 2005, 2006; Nakazawa et al., 2004; Norris et al., 2004, 2005; Suzuki et al., 2004; Kern et al., 2005; Lindsley et al., 2005; Nakamura et al., 2005; Rios et al., 2005; Kii et al., 2006]. In this report, we utilize newly developed reagents: (i) periostin knockout mice, (ii) periostin specific antibodies, and (iii) periostin adenoviruses to examine the possibility that collagen I fibrillogenesis and mechanical properties of connective tissues are dependent on the presence of periostin protein.

Colocalization of Periostin and Collagen

IHC demonstrates strong expression of periostin in adult mice valve leaflets and their suspensory apparatus such as chordae tendineae (Fig. 2B,C). Not surprisingly, these same structures express high levels of collagen (Fig. 2A). Similar co-expression patterns are evident in other fibrous connective tissue subjected to mechanical stress such as skin (Figs. 1 and 2D), tendon and PDLs (not shown). Thus, at the microscopic level, IHC demonstrates colocalization of periostin and collagen Type I. In order to further investigate periostin and collagen I co-localization at the ultrastructural level we performed immunogold IHC using specific α-mouse periostin antibodies. TEM
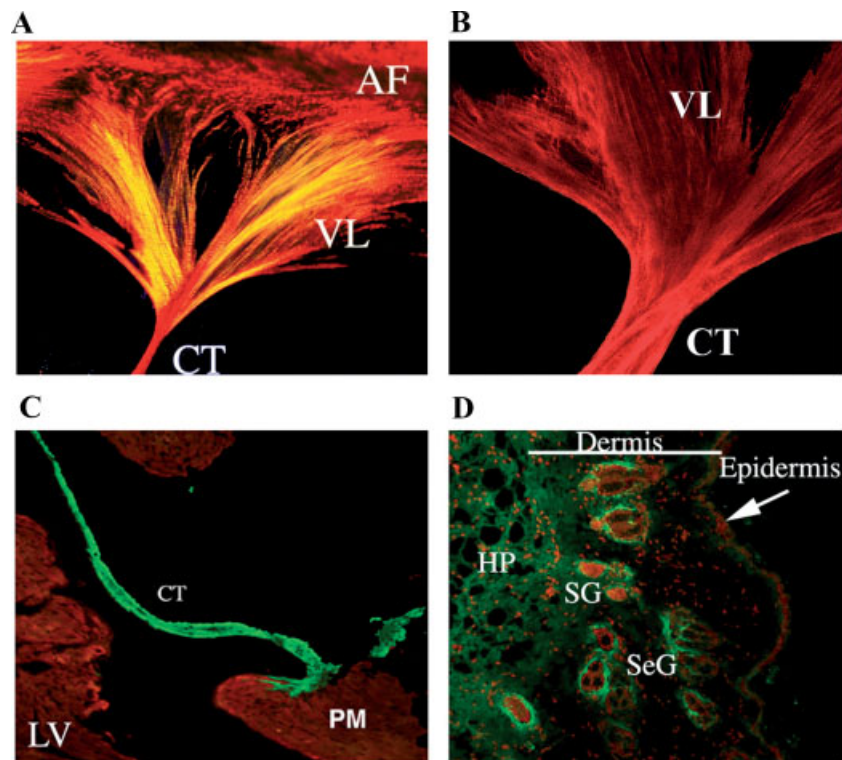
Fig. 2. Collagen and Periostin expression in adult mouse heart valve and skin. **A**: The entire left AV valve leaflet was micro-dissected from an adult mouse heart and stained for collagen using picrosirius red. Collagen expression is seen throughout the valve leaflet (VL), the chordae tendineae (CT) and annulus fibrosae (AF). The intense red staining indicates mature collagen fibers whereas the yellow stain shows less highly cross-linked fibers. **B**: The murine left AV valve leaflet was microdissected and stained in whole mount for periostin. Notice the extensive overlap in expression between periostin and collagen. **C**: Periostin expression in the adult mouse heart valve. Immunohisto-chemistry of a frontal section through an adult heart stained for periostin expression shows intense expression (green staining) within the chordae tendineae (CT). No expression is evident in the muscular left ventricle (LV) or in the papillary muscle (PM). MF20 staining was used to stain muscle (red staining). **D**: Immunostaining of periostin in adult mouse skin. Periostin (green staining) expression is seen throughout the various layers of the skin and is concentrated in areas surrounding the sebaceous glands (SeG) and the sweat glands (SG); HP-hypodermis.

studies of adult mouse AV valve leaflets found that periostin decorates collagen fibrils. Note the electron dense gold conjugates in Figure 3B. These conjugates were not observed in the no primary, negative controls (Fig. 3A).

Periostin Binds to Collagen Type I

To further elucidate whether periostin is able to directly interact with collagen I, as suggested by the immunogold TEMs, bio-chemical co-immunoprecipitation experiments were performed using immobilized collagen I. Eukaryotically expressed periostin was found to co-precipitate with collagen Type I indicating a direct, specific protein–protein interaction (Fig. 4A-arrows, B–asterisks). Six negative controls and one positive control experiment were performed to confirm the specificity of the interaction (Fig. 4A). This is the first demonstration of direct binding of periostin to collagen Type I.

Reduced Diameter of Collagen Fibrils in Periostin Knockout Mice

To determine if periostin has an effect on collagen fibrillogenesis, collagen fibril diameter and distribution in skin and tendon of periostin knockout and wild-type mice were investigated. Alterations or redistribution of collagen fibrils is used as an indicator of aberrant collagen fibrillogenesis [Christiansen et al., 2000]. Figure 5A, B shows that periostin knockout mice have a significant reduction in collagen fibril diameter indicating aberrant collagen fibril organization. In addition, the knockout mice exhibited a substantial reduction in the
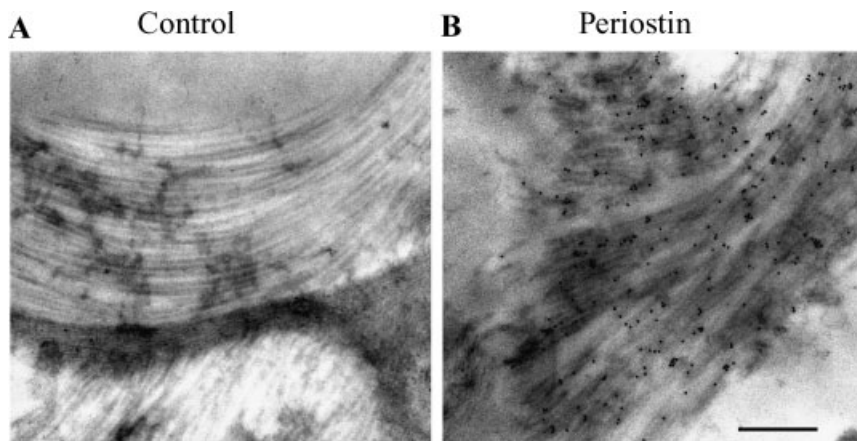
Fig. 3. Immunogold transmission electron microscopic localization of periostin along collagen fibrils. Transverse sections of the left anterior AV valve leaflet from an adult mouse were assayed for the presence of periostin using immunogold TEM. **A**: No primary antibody control immunogold TEM showing no gold particles on the collagen fibers. **B**: Electrondense gold particles (immunogold positive dots) were localized to collagen fibrils using the anti-mouse periostin anti-sera; (Bar = 500 nm).
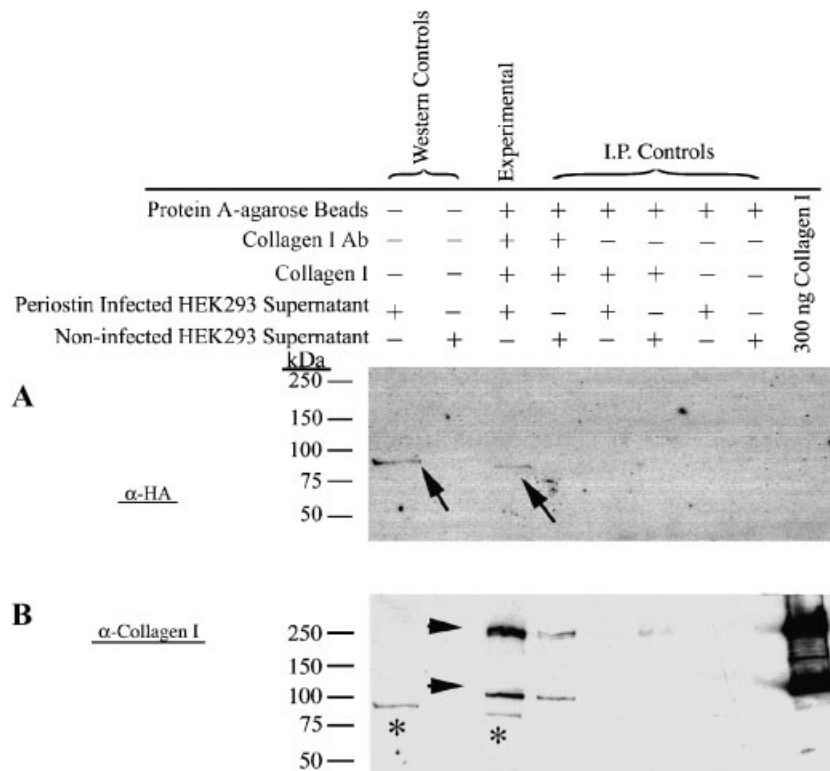

Fig. 4. Co-Immunoprecipitation of Periostin with Collagen I. Denatured immunoprecipitated complexes were electrophoresed and immunoblotted using either an anti-HA antibody (specific for adenovirally produced periostin) (**A**) or an anti-collagen I antibody (**B**). Arrows in A (and asterisks in B) signify a positive, specific interaction with collagen type I (experimental lane). All of the negative controls (represented by I.P. controls) are negative. Positive and negative controls for the HA Western is indicated (Western Controls). To ensure that collagen I is present in the experimental lane, a reprobing of the same blot using an anti-collagen I antibody was performed. As expected, collagen immunoreactive bands are represented (arrow heads). Molecular weights are depicted at the left side of the panels.
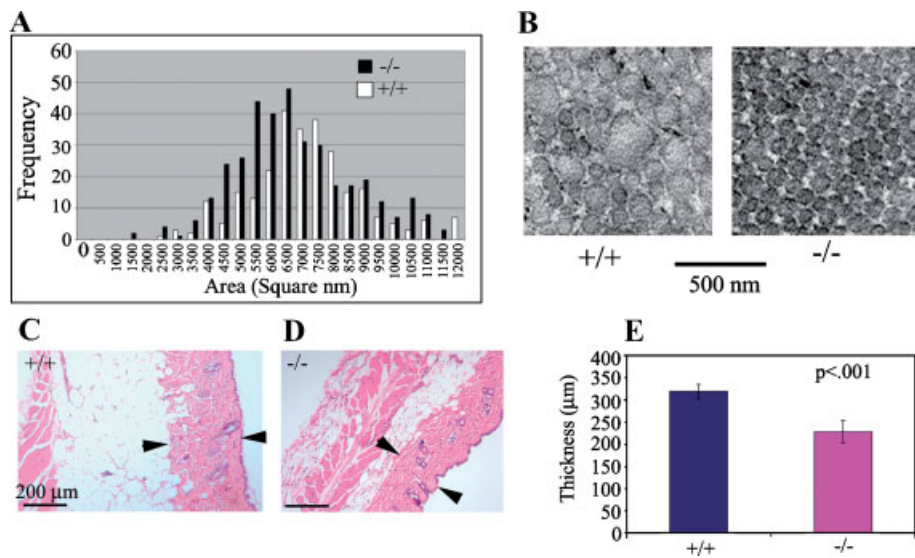
Fig. 5. Altered distribution of collagen fibril diameter in periostin knockout and wild-type mice. **A:** Collagen fibril diameter was measured using NIH image as described in Materials and Methods section. A shift to the left indicates a decrease in collagen fibril diameter. **B:** Transmission electron micrograph of collagen fibrils from periostin knockout (−/−) and wild-type (+/+) mouse skin. Notice the decrease in fibril diameter. **C, D:** Hematoxylin and Eosin (H&E) staining of skin samples from wild-type (+/+) and knock-out (−/−) mice. Arrow heads denote the boundaries of the collagenous dermal layer and signifies points at which measurements were conducted. **E:** Graphical representations of measurements made from H&E stained sections. Notice a significant decrease in the thickness of the dermis is evident in the periostin knockout mice.

thickness of the collagenous dermal layer of the skin (Fig. 5C–E).

Decreased Collagen Cross-Linking in Periostin Knockout Mice

To determine if the level of collagen cross-linking was also altered in periostin knockout mice, DSC was performed. This system evaluates denaturation of tissue samples in $5°C$ increments and therefore is a direct measure of collagen cross-linking. Freshly isolated tendon from five periostin knockout mice and five wild-type mice were used. Periostin knockout mice exhibited a reduction in the denaturation temperature of collagen (Fig. 6). Representative DSC profiles of tendon samples from wild-type and periostin knockout mice are presented in Figure 6A. Thermal denaturing temperatures were statistically different from wild-type mice as shown in Figure 6B. Since thermal denaturation temperature reflects the level of collagen cross-linking [Miles et al., 2005; Pietrucha, 2005], these data strongly indicate a reduced level of collagen cross-linking in periostin knockout mice and therefore is consistent with periostin regulating collagen fibril assembly and maturation.

Characterization of Mechanical Properties of Skin in Periostin Knockout Mice

A typical experiment derived from stretching fresh dorsal skin from two animals is shown in Figure 7A. The stress−strain relationship for all
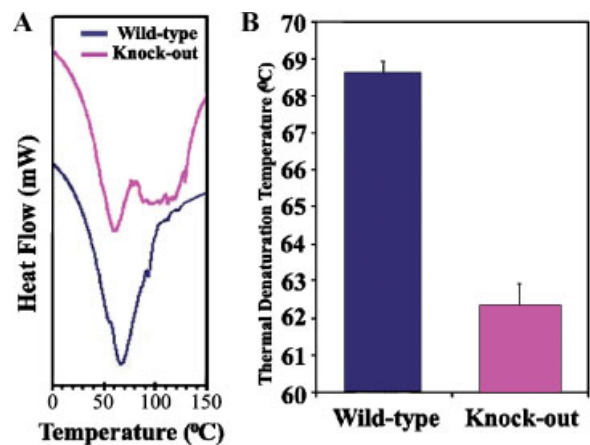

Fig. 6. Collagen cross-linking is reduced in the periostin null mouse. **A:** Representative differential scanning calorimetry (DSC) profiles of tendon samples from wild-type and periostin null mice. **B:** Thermal denaturation temperatures of wild-type and periostin null mice. Lower denaturation temperatures for null mice indicate reduced collagen cross-linking.
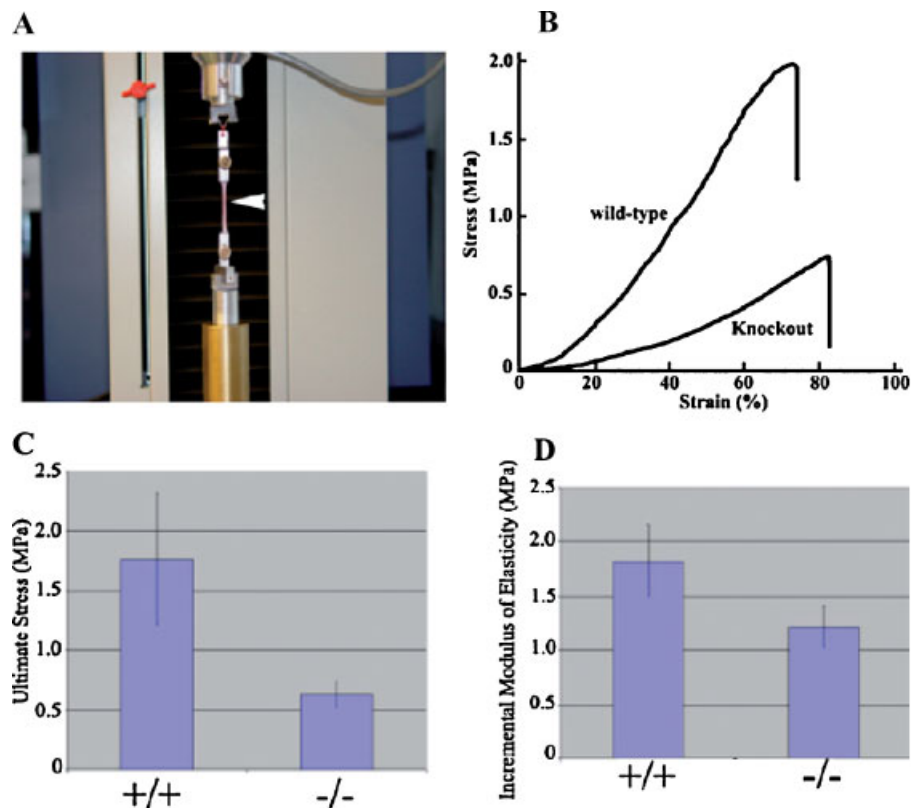
Fig. 7. Skin from adult periostin null mice have reduced tensile strength. **A**: Tensile test experimentation machine. **B**: Typical stress–strain relationship for adult skin sample from wild-type (+/+) and periostin null (−/−). **C**: Quantitative comparison of ultimate stress between the dorsal skin of wild-type (+/+) and periostin null (−/−). **D**: Quantitative comparison between the incremental modulus of elasticity (at the stress levels between 0.25 and 0.30 MPa) between wild-type (+/+) and periostin null (−/−) skin.

skin specimens was non-linear. However, skin from the knockout mouse exhibited lower tensile strength in contrast with the skin from the wild-type. Incremental modulus of elasticity (at the stress level 0.25/0.3 MPa) of dorsal skin samples of the wild-type and knockout mice were statistically different from each another: 1.82 ± 0.32 and 1.21 ± 0.19 MPa, respectively ($P < 0.05$). In addition, skin from knockout mice exhibited a substantially lower ultimate stress (Fig. 7B) than that seen with the wild-type mice: 0.63 ± 0.10 and 1.77 ± 0.55 MPa, respectively ($P < 0.05$). Therefore, the skin from wild-type mice is stiffer than that from knockout mice, demonstrating the absence of periostin causes an increase in skin compliance.

Infection With Periostin Adenoviruses Alters the Visco-Elastic Properties of Mesenchymal Valve Tissue

If periostin has a direct effect on the mechanical properties of connective tissues, then altering levels of periostin expression in these tissues should result in biomechanical changes. In our preliminary studies it was shown that mechanical properties of cushion tissue (tissue surface tension and viscosity) are regulated during development (Damon et al. unpublished observations). At HH27, a time point of intense periostin expression, the valve mesenchymal tissue is sufficient in size to perform tensiometric assays and tissue fusion assays. Data generated from these assays were used to calculate the visco-elastic properties of embryonic prevalvular mesenchymal tissues.

Tensiometric Studies

In order to assay the affect periostin has on the biomechanics of connective tissues, a periostin overexpressing adenovirus was constructed as shown in Figure 8A. This virus (and a LacZ control adenovirus) was functionally evaluated in HEK293 cells to ensure extracellular secretion (Fig. 8B). Western blot
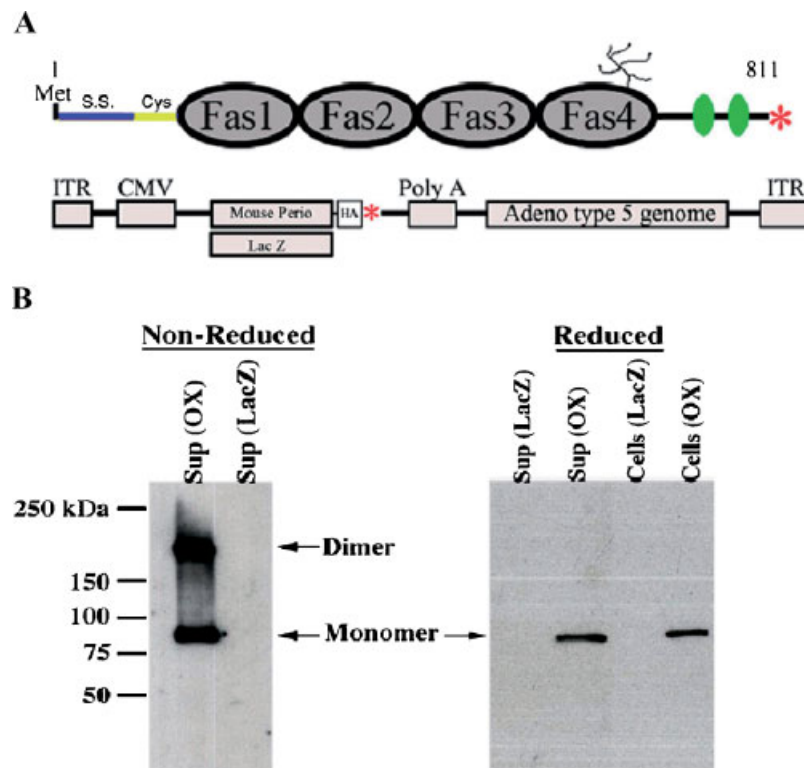
Fig. 8. Validation of periostin virus. **A**: Schematic of Periostin showing the fasciclin domains (Fas1-4), signal sequence (S.S.), cysteine rich domain (Cys), heparin binding domain (green ovals), putative glycosylation site, and stop codon (red asterisk). Below the periostin schematic is a representation of the two adenoviruses (LacZ and mouse periostin) generated for experimentation (HA-hemagluttinin epitope tag fused at the carboxyl-terminus of periostin, ITR-Internal terminal repeat, CMV-cytomegalovirus promoter, red asterisk-stop codon). **B**: Western blot for periostin (OX) or LacZ adenoviral infected HEK293 cells under reducing (with β-mercaptoethanol: β-ME) or non-reducing conditions (without β-ME). Under non-reducing conditions, periostin migrates as both a monomer and a dimer and is capable of being secreted into the supernatant. Periostin is also seen still attached to the cells, suggesting its ability to be matricellular.

analysis confirms the ability for periostin to be secreted as well as the ability to homodimerize. These adenoviruses were then used in tensiometry experiments with cardiac valve tissue.

Tensiometry measurements on isolated rounded cushion explants were performed using the apparatus shown in Figure 10A. Infectability of AV cushions in hanging drops was initially assessed by infecting the tissue with GFP and periostin adenoviruses. These tissues are able to be infected as demonstrated by immunofluorescence and Western blotting (Fig. 9A,B). Following infection of the mouse periostin adenovirus, surface tension was not appreciably affected (Fig. 10B). In order to estimate tissue viscosity, tissue fusion assays were performed (Fig. 10C,D). Kinetics of tissue fusion of two opposing rounded mesenchymal tissue aggregates allowed calculation of the ratio of tissue surface tension to tissue viscosity (Fig. 10C). This ratio, combined with data on direct measurements of tissue surface tension (estimated by tensiometry) was further used to calculate tissue viscosity. Data demonstrate that overexpression of periostin increased tissue viscosity (Fig. 10D). To validate that these results were specific to periostin and not a non-specific adenovirus affect, tissue aggregates were also infected with a LacZ control adenovirus. Incubation with the LacZ adenovirus generated statistically similar values as observed with the non-infected controls (Fig. 10B–D). This demonstrates that the differences obtained in tissue fusion and viscosity are specific for periostin overexpression and not due to non-specific adenovirus affects. To the best of our knowledge, this is the first report providing direct evidence that the viscosity of mesenchymal connective tissues is regulated in part by periostin.
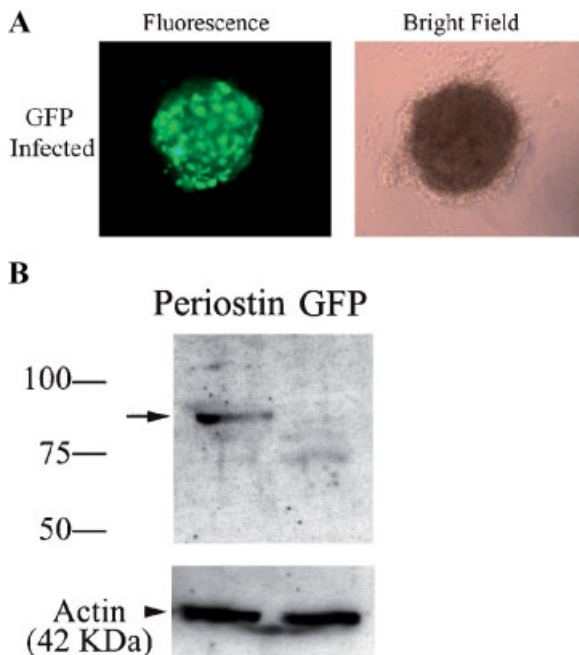
A   Fluorescence   Bright Field

GFP
Infected

B

Periostin GFP

100—

75—

50—

Actin
(42 KDa)

Fig. 9. HH27 AV cushion infectability To verify that HH27 AV cushions in hanging drops are amenable to infection, the GFP and periostin adenoviruses were added to the cultures. **A**: Immunofluorescence verified infection and expression of the GFP adenovirus. **B**: Western blotting (using an anti-HA antibody) was performed to further confirm the infection of adenovirally produced periostin. The arrow shows immunopositive periostin expression thereby validating the adenovirus infection and expression in H27 AV cushion hanging drop cultures. Actin was used to verify equal loading.

DISCUSSION

Connective tissues such as skin, tendon, and heart valves are rich in collagens and fasciclin proteins (periostin and βIG-H3). The primary structural component conferring most biomechanical and material properties to connective tissues is collagen Type I. Therefore, we aimed to examine the potential molecular interaction of periostin with collagen Type I, and the impact it might have on the material properties of connective tissues. In this study, we report the co-localization of periostin and collagen Type I as seen by IHC and transmission electron microscopy in murine skin and heart valves. Most importantly, we biochemically defined a direct interaction between periostin and collagen Type I. This is the first known report demonstrating periostin–collagen Type I interactions. This interaction was also observed at the electron microscopic level. Immunogold transmission electron microscopy of adult mouse heart valves demonstrated the presence of periostin on collagen fibrils. This coincides with previously reported co-localization of periostin and collagen in the PDL [Suzuki et al., 2004; Kii et al., 2006]. Taken together, these data strongly indicate a molecular interaction between periostin and collagen Type I. Recently, additional ECM components such as tenascin-C, fibronectin, and collagen V have been shown to interact with periostin
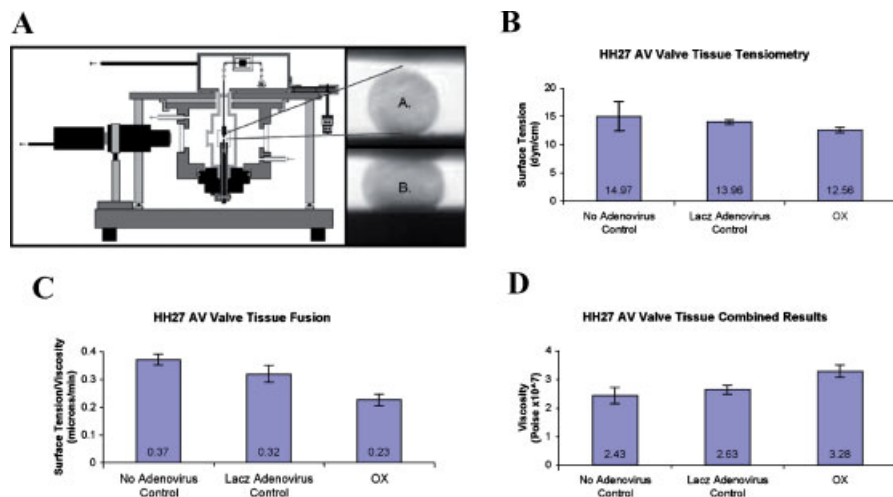

Fig. 10. Periostin increases the visco-elastic properties of HH27 atrioventricular mesenchymal valve tissue. **A**: Schematic illustration of the tensiometer (not to scale), A and B correspond, respectively, to uncompressed and compressed valve explants. **B**: Tensiometry measurements of rounded cushion explants showing no statistical change in surface tension when periostin is overexpressed (OX). **C**: Fusion assays demonstrating periostin overexpression (OX) decreases the rate (proportional to the ratio of surface tension to viscosity) at which valve explants fuse. **D**: Statistically significant increase in viscosity of HH27 valve explants when periostin is overexpressed (OX).

[Takayama et al., 2006]. How these interactions are functionally important remains to be seen. More importantly, the identification of specific collagen I, tenascin-C, fibronectin, and collagen V binding domains within the periostin molecule will be an essential step in understanding how these proteins organize in the ECM.

Although we demonstrate, through molecular and biochemical approaches, that periostin binds specifically to collagen I both in vivo and in vitro, it is important to link these interactions to mechanistic function at the tissue and organ level. In this report we present novel biomechanical data that demonstrates the importance of periostin in collagen fibrillogenesis, ultimately dictating structural integrity and functional consequences in connective tissues such as skin, tendon, and heart valves.

Collagen fibrillogenesis is a multistep process which involves linear and accelerative growth followed by lateral growth and subsequent collagen fiber fusion [Kadler et al., 1996; Berisio et al., 2002; Canty and Kadler, 2002, 2005; Hulmes, 2002; Silver et al., 2003; Kadler, 2004]. Based on studies of collagen fibrillogenesis in vitro it has been suggested that there is a correlation between collagen fibril diameter and mechanical properties of collagen-based connective tissues [Christiansen et al., 2000]. By altering collagen diameter, the structural and functional integrity of the connective tissue is compromised. Morphometric studies of transmission electron micrographs of ultrathin skin sections demonstrate reduced diameter of collagen fibrils in periostin knockout mice compared to wild-type mice. Thus, this alteration reflects defects in collagen fibril maturation and assembly. Mechanistically this may occur through specific periostin−collagen interactions which bridge and stabilize adjacent collagen fibrils during fibril fusion. This theory is supported by three key pieces of data: (i) periostin binds directly to collagen Type I fibrils, (ii) periostin null mice exhibit a reduction in fibril diameter, and (iii) periostin null mice have a reduction in collagen cross linking as determined by DSC. Similar results have been obtained in the context of Sparc (secreted protein acidic rich cystein, also known as osteonectin and BM-40) deficient animals [Bradshaw et al., 2003]. Collagen fibril diameter and collagen cross-linking are decreased in these animals and result in alterations in the biomechanical properties of connective tissues.

The mechanisms by which Sparc effects collagen fibril diameter may be through the direct binding to collagen Type I. Additionally, Sparc is a substrate for transglutaminase, an enzyme that establishes cross-links between proteins [Aeschlimann et al., 1995]. It is unclear at the present whether periostin is a substrate for this enzyme or other enzymes involved in cross-linking collagen moieties (such as lysyl oxidase). However, it is not unreasonable to hypothesize that periostin may be a substrate for one of these cross-linking enzymes, thus mechanistically explaining the duality of periostin function during collagen fibrillogenesis.

The extrapolation of mechanical properties of connective tissues from the analysis of collagen diameter distribution is an important initial step in understanding the contribution of periostin to collagen fibrillogenesis. However, to fully appreciate the significance periostin may play in regulating and maintaining proper biomechanics of connective tissues, additional assays must be employed which examine specific biomechanical parameters when periostin expression is altered. To address these concerns, two main biomechanical experiments were developed and applied to cell and tissue specific assays. First, overexpression of periostin in isolated rounded embryonic chick heart mesenchymal valve tissue explants resulted in increased tissue viscosity as measured by using surface tensiometry and tissue fusion assays. Mechanisms by which this occurs are currently being evaluated and may involve induction of procollagen expression, enhanced fibril maturation and stabilization, and/or resistance to the natural process of collagen fibril turnover. In addition, we have recently shown that periostin, through integrin signaling, enhances collagen contraction in embryonic mesenchymal valve tissue [Butcher et al., 2006], further substantiating a role for periostin in the regulation of matrix strength and integrity. Second, an analysis of skin compliance in the context of the periostin null mouse would provide important information on the role that periostin may play in responding to increasing amounts of biomechanical forces (i.e., stress and strain relationship). These experiments demonstrate that the skin of wild-type mice is stiffer (less compliant) than skin of the periostin knockout mouse—incremental modulus of elasticity of dorsal skin samples of the wild-type mice is

higher than the skin from knockout mice. The skin specimen from the wild-type mice exhibited higher ultimate stress in contrast with the skin from the knockout type. In addition, the data generated from these skin samples suggest that periostin knockout mice develop a skin hyperextensive syndrome or "cutis laxa" similar to what is seen in patients with the collagen associated EDS [Judd, 1984; Uitto and Shamban, 1987; Tsukahara et al., 1988; Gorlin and Cohen, 1989].

Collectively, the molecular, biochemical, and biomechanical data provide important insights into the mechanisms of periostin function at the tissue level. In light of this data and due to strong expression of periostin in heart valves and their tendinous supporting structures (chordae tendineae) it will be important to evaluate the periostin null mice for cardiovascular defects. These potential defects would stem from altered formation and remodeling of the cardiac valves, which would compromise their ability to withstand extensive hemodynamic stresses during the cardiac contraction cycle. Developmental defects in the ECM can have major implications that over time greatly affect valve function. Thus, even small changes in the composition (and alignment) of the valvular ECM can, over time, compromise valve integrity and result in valvular and cardiovascular diseases (i.e., ECM changes over time = pathology). This is evident in Marfan Syndrome (Fibrillin-1 mutations) [Wang et al., 1996; Bonnet et al., 1997; Milewicz, 1998; von Kodolitsch et al., 1998; Pyeritz, 2000; Loeys et al., 2001; Elcioglu et al., 2004] and EDS (*COL5A1, COL5A2, and COL1A2* mutations with involvement of tenascin-X, and *COL1A1*) [Scarbrough et al., 1984; Tsukahara et al., 1988; Loughlin et al., 1995; Burrows et al., 1996; Bonnet et al., 1997; Milewicz, 1998; Peeters et al., 2004; Schwarze et al., 2004; Lindor and Bristow, 2005]. As is the case for both Marfan Syndrome and EDS, valve abnormalities result in mitral, tricuspid and/or aortic valve prolapse, regurgitation, aortic aneurism, and a host of secondary cardiac defects (ventricular hypertrophy, cardiac arrhythmia's, and heart failure). Of potential clinical significance, EDS type II syndrome has been associated with an unbalanced (6q;13q) translocation which includes the locus for periostin at 13q13.3 [Scarbrough et al., 1984]. In addition, patients with Rieger syndrome type II, (who have

assorted cardiovascular malformations such as: aortic valvular stenosis, inter-atrial defects, congenital tricuspid valve anomaly, bicuspid aortic valve, etc.) have been assigned to chromosomal break points near the periostin locus [Stathacopoulos et al., 1987; Phillips et al., 1996; Mammi et al., 1998].

In conclusion, the data presented in this report define, for the first time, that periostin can regulate collagen fibrillogenesis and is essential to the biomechanical properties of connective tissues such as skin, tendon, and the heart valves. In addition, the periostin null mouse may be a useful model for understanding molecular, cellular, and biomechanical mechanisms of various connective tissue diseases in humans.

REFERENCES

Aeschlimann D, Kaupp O, Paulsson M. 1995. Transglutaminase—Catalyzed matrix cross-linking in differentiating cartilage: Identification of osteonectin as a major glutaminyl substrate. J Cell Biol 129:881–892.

Ameye L, Young MF. 2002. Mice deficient in small leucine-rich proteoglycans: Novel in vivo models for osteoporosis, osteoarthritis, Ehlers-Danlos syndrome, muscular dystrophy, and corneal diseases. Glycobiology 12:107R–116R.

Ameye L, Aria D, Jepsen K, Oldberg A, Xu T, Young MF. 2002. Abnormal collagen fibrils in tendons of biglycan/fibromodulin-deficient mice lead to gait impairment, ectopic ossification, and osteoarthritis. FASEB J 16:673–680.

Beck GR, Jr., Moran E, Knecht N. 2003. Inorganic phosphate regulates multiple genes during osteoblast differentiation, including Nrf2. Exp Cell Res 288:288–300.

Berisio R, Vitagliano L, Mazzarella L, Zagari A. 2002. Recent progress on collagen triple helix structure, stability and assembly. Protein Pept Lett 9:107–116.

Birk DE, Trelstad RL. 1986. Extracellular compartments in tendon morphogenesis: Collagen fibril, bundle, and macroaggregate formation. J Cell Biol 103:231–240.

Bonnet D, Saygili A, Bonhoeffer P, Fermont L, Sidi D, Kachaner J. 1997. Atrio-ventricular valve dysplasia in 22 newborn infants. Int J Cardiol 59:113–118.

Bornstein P, Armstrong LC, Hankenson KD, Kyriakides TR, Yang Z. 2000. Thrombospondin 2, a matricellular protein with diverse functions. Matrix Biol 19:557–568.

Bradshaw AD, Puolakkainen P, Dasgupta J, Davidson JM, Wight TN, Helene Sage E. 2003. SPARC-null mice display abnormalities in the dermis characterized by decreased collagen fibril diameter and reduced tensile strength. J Invest Dermatol 120:949–955.

Burrows NP, Nicholls AC, Yates JR, Gatward G, Sarathachandra P, Richards A, Pope FM. 1996. The gene encoding collagen alpha1(V)(COL5A1) is linked to mixed Ehlers-Danlos syndrome type I/II. J Invest Dermatol 106:1273–1276.

Butcher JT, Norris RA, Hoffman S, Mjaatvedt CH, Markwald RR. 2006. Periostin promotes atrioventricular mesenchyme matrix invasion and remodeling mediated by integrin signaling through Rho/PI 3-Kinase. Dev Biol [Epub ahead of print].

Canty EG, Kadler KE. 2002. Collagen fibril biosynthesis in tendon: A review and recent insights. Comp Biochem Physiol A Mol Integr Physiol 133:979–985.

Canty EG, Kadler KE. 2005. Procollagen trafficking, processing and fibrillogenesis. J Cell Sci 118:1341–1353.

Chakravarti S. 2002. Functions of lumican and fibromodulin: Lessons from knockout mice. Glycoconj J 19:287–293.

Christiansen DL, Huang EK, Silver FH. 2000. Assembly of type I collagen: Fusion of fibril subunits and the influence of fibril diameter on mechanical properties. Matrix Biol 19:409–420.

Elcioglu NH, Akalin F, Elcioglu M, Comeglio P, Child AH. 2004. Neonatal Marfan syndrome caused by an exon 25 mutation of the fibrillin-1 gene. Genet Couns 15:219–225.

Ezura Y, Chakravarti S, Oldberg A, Chervoneva I, Birk DE. 2000. Differential expression of lumican and fibromodulin regulate collagen fibrillogenesis in developing mouse tendons. J Cell Biol 151:779–788.

Forgacs G, Foty RA, Shafrir Y, Steinberg MS. 1998. Viscoelastic properties of living embryonic tissues: A quantitative study. Biophys J 74:2227–2234.

Foty RA, Pfleger CM, Forgacs G, Steinberg MS. 1996. Surface tensions of embryonic tissues predict their mutual envelopment behavior. Development 122:1611–1620.

Frenkel J. 1945. Viscous flow of crystalline bodies under the action of surface tension. J Phys (Moscow) 9:385–391.

Goldberg M, Septier D, Oldberg A, Young MF, Ameye LG. 2006. Fibromodulin-deficient mice display impaired collagen fibrillogenesis in predentin as well as altered dentin mineralization and enamel formation. J Histochem Cytochem 54:525–537.

Gorlin RJ, Cohen MM, Jr. 1989. Craniofacial manifestations of Ehlers-Danlos syndromes, cutis laxa syndromes, and cutis laxa-like syndromes. Birth Defects Orig Artic Ser 25:39–71.

Hamburger V, Hamilton HL. 1951. A series of normal stages in the development of the chick. J Morphol 8:49–92.

Horiuchi K, Amizuka N, Takeshita S, Takamatsu H, Katsuura M, Ozawa H, Toyama Y, Bonewald LF, Kudo A. 1999. Identification and characterization of a novel protein, periostin, with restricted expression to periosteum and periodontal ligament and increased expression by transforming growth factor beta. J Bone Miner Res 14:1239–1249.

Hulmes DJ. 2002. Building collagen molecules, fibrils, and suprafibrillar structures. J Struct Biol 137:2–10.

Judd KP. 1984. Hyperelasticity syndromes. Cutis 33:494–496.

Kadler K. 2004. Matrix loading: Assembly of extracellular matrix collagen fibrils during embryogenesis. Birth Defects Res C Embryo Today 72:1–11.

Kadler KE, Holmes DF, Trotter JA, Chapman JA. 1996. Collagen fibril formation. Biochem J 316(Pt 1):1–11.

Katsuragi N, Morishita R, Nakamura N, Ochiai T, Taniyama Y, Hasegawa Y, Kawashima K, Kaneda Y, Ogihara T, Sugimura K. 2004. Periostin as a novel factor responsible for ventricular dilation. Circulation 110:1806–1813.

Kern CB, Hoffman S, Moreno R, Damon BJ, Norris RA, Krug EL, Markwald RR, Mjaatvedt CH. 2005. Immunolocalization of chick periostin protein in the developing heart. Anat Rec A Discov Mol Cell Evol Biol 284:415–423.

Kii I, Amizuka N, Minqi L, Kitajima S, Saga Y, Kudo A. 2006. Periostin is an extracellular matrix protein required for eruption of incisors in mice. Biochem Biophys Res Commun 342:766–772.

Kruzynska-Frejtag A, Machnicki M, Rogers R, Markwald RR, Conway SJ. 2001. Periostin (an osteoblast-specific factor) is expressed within the embryonic mouse heart during valve formation. Mech Dev 103:183–188.

Kruzynska-Frejtag A, Wang J, Maeda M, Rogers R, Krug E, Hoffman S, Markwald RR, Conway SJ. 2004. Periostin is expressed within the developing teeth at the sites of epithelial-mesenchymal interaction. Dev Dyn 229:857–868.

Kudo H, Amizuka N, Araki K, Inohaya K, Kudo A. 2004. Zebrafish periostin is required for the adhesion of muscle fiber bundles to the myoseptum and for the differentiation of muscle fibers. Dev Biol 267:473–487.

Kyriakides TR, Zhu YH, Smith LT, Bain SD, Yang Z, Lin MT, Danielson KG, Iozzo RV, LaMarca M, McKinney CE, Ginns EI, Bornstein P. 1998. Mice that lack thrombospondin 2 display connective tissue abnormalities that are associated with disordered collagen fibrillogenesis, an increased vascular density, and a bleeding diathesis. J Cell Biol 140:419–430.

Li S, Van Den Diepstraten C, D'Souza SJ, Chan BM, Pickering JG. 2003. Vascular smooth muscle cells orchestrate the assembly of type I collagen via alpha2-beta1 integrin, RhoA, and fibronectin polymerization. Am J Pathol 163:1045–1056.

Li G, Oparil S, Sanders JM, Zhang L, Dai M, Chen LB, Conway SJ, McNamara CA, Sarembock IJ. 2005. Phosphatidylinositol-3-kinase signaling mediates vascular smooth muscle cell expression of periostin in vivo and in vitro. Atherosclerosis 188:292–300.

Lindner V, Wang Q, Conley BA, Friesel RE, Vary CP. 2005. Vascular injury induces expression of periostin: Implications for vascular cell differentiation and migration. Arterioscler Thromb Vasc Biol 25:77–83.

Lindor NM, Bristow J. 2005. Tenascin-X deficiency in autosomal recessive Ehlers-Danlos syndrome. Am J Med Genet Part A 135A:75–80.

Lindsley A, Li W, Wang J, Maeda N, Rogers R, Conway SJ. 2005. Comparison of the four mouse fasciclin-containing

genes expression patterns during valvuloseptal morphogenesis. Gene Expr Patterns 5:593–600.

Litvin J, Selim AH, Montgomery MO, Lehmann K, Rico MC, Devlin H, Bednarik DP, Safadi FF. 2004. Expression and function of periostin-isoforms in bone. J Cell Biochem 92:1044–1061.

Litvin J, Zhu S, Norris R, Markwald R. 2005. Periostin family of proteins: Therapeutic targets for heart disease. Anat Rec A Discov Mol Cell Evol Biol 287:1205–1212.

Litvin J, Blagg A, Mu A, Matiwala S, Montgomery M, Berretta R, Houser S, Margulies K. 2006. Periostin and periostin-like factor in the human heart: Possible therapeutic targets. Cardiovasc Pathol 15:24–32.

Loeys B, Nuytinck L, Delvaux I, De Bie S, De Paepe A. 2001. Genotype and phenotype analysis of 171 patients referred for molecular study of the fibrillin-1 gene FBN1 because of suspected Marfan syndrome. Arch Intern Med 161:2447–2454.

Loughlin J, Irven C, Hardwick LJ, Butcher S, Walsh S, Wordsworth P, Sykes B. 1995. Linkage of the gene that encodes the alpha 1 chain of type V collagen (COL5A1) to type II Ehlers-Danlos syndrome (EDS II). Hum Mol Genet 4:1649–1651.

Mammi I, De Giorgio P, Clementi M, Tenconi R. 1998. Cardiovascular anomaly in Rieger Syndrome: Heterogeneity or contiguity? Acta Ophthalmol Scand 76:509–512.

Matheson S, Larjava H, Hakkinen L. 2005. Distinctive localization and function for lumican, fibromodulin and decorin to regulate collagen fibril organization in periodontal tissues. J Periodontal Res 40:312–324.

Miles CA, Avery NC, Rodin VV, Bailey AJ. 2005. The increase in denaturation temperature following cross-linking of collagen is caused by dehydration of the fibres. J Mol Biol 346:551–556.

Milewicz DM. 1998. Molecular genetics of Marfan syndrome and Ehlers-Danlos type IV. Curr Opin Cardiol 13:198–204.

Minamitani T, Ariga H, Matsumoto K. 2004a. Deficiency of tenascin-X causes a decrease in the level of expression of type VI collagen. Exp Cell Res 297:49–60.

Minamitani T, Ikuta T, Saito Y, Takebe G, Sato M, Sawa H, Nishimura T, Nakamura F, Takahashi K, Ariga H, Matsumoto K. 2004b. Modulation of collagen fibrillogenesis by tenascin-X and type VI collagen. Exp Cell Res 298:305–315.

Nakamura S, Terashima T, Yoshida T, Iseki S, Takano Y, Ishikawa I, Shinomura T. 2005. Identification of genes preferentially expressed in periodontal ligament: Specific expression of a novel secreted protein, FDC-SP. Biochem Biophys Res Commun 338:1197–1203.

Nakazawa T, Nakajima A, Seki N, Okawa A, Kato M, Moriya H, Amizuka N, Einhorn TA, Yamazaki M. 2004. Gene expression of periostin in the early stage of fracture healing detected by cDNA microarray analysis. J Orthop Res 22:520–525.

Norris RA, Kern CB, Wessels A, Moralez EI, Markwald RR, Mjaatvedt CH. 2004. Identification and detection of the periostin gene in cardiac development. Anat Rec A Discov Mol Cell Evol Biol 281:1227–1233.

Norris RA, Kern CB, Wessels A, Wirrig EE, Markwald RR, Mjaatvedt CH. 2005. Detection of betaig-H3, a TGFbeta induced gene, during cardiac development and its

complementary pattern with periostin. Anat Embryol (Berl) 210:13–23.

Oshima A, Tanabe H, Yan T, Lowe GN, Glackin CA, Kudo A. 2002. A novel mechanism for the regulation of osteoblast differentiation: Transcription of periostin, a member of the fasciclin I family, is regulated by the bHLH transcription factor, twist. J Cell Biochem 86:792–804.

Peeters AC, Kucharekova M, Timmermans J, van den Berkmortel FW, Boers GH, Novakova IR, Egging D, den Heijer M, Schalkwijk J. 2004. A clinical and cardiovascular survey of Ehlers-Danlos syndrome patients with complete deficiency of tenascin-X. Neth J Med 62:160–162.

Phillips JC, del Bono EA, Haines JL, Pralea AM, Cohen JS, Greff LJ, Wiggs JL. 1996. A second locus for Rieger syndrome maps to chromosome 13q14. Am J Hum Genet 59:613–619.

Pietrucha K. 2005. Changes in denaturation and rheological properties of collagen-hyaluronic acid scaffolds as a result of temperature dependencies. Int J Biol Macromol 36:299–304.

Pyeritz RE. 2000. The Marfan syndrome. Annu Rev Med 51:481–510.

Rios H, Koushik SV, Wang H, Wang J, Zhou HM, Lindsley A, Rogers R, Chen Z, Maeda M, Kruzynska-Frejtag A, Feng JQ, Conway SJ. 2005. Periostin null mice exhibit dwarfism, incisor enamel defects, and an early-onset periodontal disease-like phenotype. Mol Cell Biol 25: 11131–11144.

Robinson PN, Arteaga-Solis E, Baldock C, Collod-Beroud G, Booms P, De Paepe A, Dietz HC, Guo G, Handford PA, Judge DP, Kielty CM, Loeys B, Milewicz DM, Ney A, Ramirez F, Reinhardt DP, Tiedemann K, Whiteman P, Godfrey M. 2006. The molecular genetics of Marfan syndrome and related disorders. J Med Genet 43: 769–787.

Sasaki H, Lo KM, Chen LB, Auclair D, Nakashima Y, Moriyama S, Fukai I, Tam C, Loda M, Fujii Y. 2001. Expression of Periostin, homologous with an insect cell adhesion molecule, as a prognostic marker in non-small cell lung cancers. Jpn J Cancer Res 92:869–873.

Scarbrough PR, Daw J, Carroll AJ, Finley SC. 1984. An unbalanced (6q;13q) translocation in a male with clinical features of Ehlers-Danlos type II syndrome. J Med Genet 21:226–228.

Schwarze U, Hata R, McKusick VA, Shinkai H, Hoyme HE, Pyeritz RE, Byers PH. 2004. Rare autosomal recessive cardiac valvular form of Ehlers-Danlos syndrome results from mutations in the COL1A2 gene that activate the nonsense-mediated RNA decay pathway. Am J Hum Genet 74:917–930.

Silver FH, Freeman JW, Seehra GP. 2003. Collagen self-assembly and the development of tendon mechanical properties. J Biomech 36:1529–1553.

Stathacopoulos RA, Bateman JB, Sparkes RS, Hepler RS. 1987. The Rieger syndrome and a chromosome 13 deletion. J Pediatr Ophthalmol Strabismus 24:198–203.

Suzuki H, Amizuka N, Kii I, Kawano Y, Nozawa-Inoue K, Suzuki A, Yoshie H, Kudo A, Maeda T. 2004. Immunohistochemical localization of periostin in tooth and its surrounding tissues in mouse mandibles during development. Anat Rec A Discov Mol Cell Evol Biol 281:1264–1275.

Takayama G, Arima K, Kanaji T, Toda S, Tanaka H, Shoji S, McKenzie AN, Nagai H, Hotokebuchi T, Izuhara K. 2006. Periostin: A novel component of subepithelial fibrosis of bronchial asthma downstream of IL-4 and IL-13 signals. J Allergy Clin Immunol 118: 98–104.

Tsukahara M, Shinkai H, Asagami C, Eguchi T, Kajii T. 1988. A disease with features of cutis laxa and Ehlers-Danlos syndrome. Report of a mother and daughter. Hum Genet 78:9–12.

Uitto J, Shamban A. 1987. Heritable skin diseases with molecular defects in collagen or elastin. Dermatol Clin 5: 63–84.

von Kodolitsch Y, Raghunath M, Nienaber CA. 1998. Marfan syndrome: Prevalence and natural course of cardiovascular manifestations. Z Kardiol 87:150–160.

Wang M, Kishnani P, Decker-Phillips M, Kahler SG, Chen YT, Godfrey M. 1996. Double mutant fibrillin-1 (FBN1) allele in a patient with neonatal Marfan syndrome. J Med Genet 33:760–763.

Whittaker P, Kloner RA, Boughner DR, Pickering JG. 1994. Quantitative assessment of myocardial collagen with picrosirius red staining and circularly polarized light. Basic Res Cardiol 89:397–410.

Wilde J, Yokozeki M, Terai K, Kudo A, Moriyama K. 2003. The divergent expression of periostin mRNA in the periodontal ligament during experimental tooth movement. Cell Tissue Res 312:345–351.

Zhang G, Ezura Y, Chervoneva I, Robinson PS, Beason DP, Carine ET, Soslowsky LJ, Iozzo RV, Birk DE. 2006. Decorin regulates assembly of collagen fibrils and acquisition of biomechanical properties during tendon development. J Cell Biochem 98:1436–1449.